

# The Two-Photon Decay Mode of MSSM Higgs Bosons at the Large Hadron Collider <sup>1</sup>

Bjarte Kileng

NORDITA, Blegdamsvej 17, DK-2100 Copenhagen Ø, Denmark

Per Osland

University of Bergen, Allégt. 55, N-5007 Bergen, Norway

and

P.N. Pandita<sup>2</sup>

Universität Kaiserslautern, Fachbereich Physik, Erwin - Schrödinger - Strasse,  
 D-67663 Kaiserslautern, Germany

## Abstract

At the Large Hadron Collider (LHC), the CP-even Higgs bosons ( $h^0$  and  $H^0$ ) of the Minimal Supersymmetric Standard Model (MSSM) will be searched for mainly through their two-photon decay. We present a detailed analysis of the production and two-photon decay of the CP-even Higgs bosons of MSSM at the LHC by taking into account all the parameters of the model, especially the bilinear parameter  $\mu$  and the trilinear supersymmetry breaking parameter  $A$ . Non-zero values of these parameters lead to significant mixing in the squark sector, and, thus, affect the masses of Higgs bosons through radiative corrections, as well as their couplings to squarks. The dependence of the cross section for the production of Higgs, and its subsequent decay to two photons, on various parameters of the MSSM is described in detail. The cross section times the two-photon branching ratio of  $h^0$  is of the order of 15–25 fb in much of the parameter space that remains after imposing the present experimental constraints on the parameters. For the  $H^0$ , the two-photon branching ratio is only significant if it is light. With a light  $H^0$  the cross section times the branching ratio may be 200 fb or more.

## 1 Introduction

In the Minimal Supersymmetric Standard Model (MSSM) [1], two Higgs doublets ( $H_1$  and  $H_2$ ) with opposite hypercharge are required in order to give masses to up- and down-quarks (leptons), and to cancel gauge anomalies. The physical Higgs boson spectrum in the MSSM consists of two CP-even neutral bosons  $h^0$  and  $H^0$ , a CP-odd neutral boson  $A^0$  and a pair of charged Higgs bosons  $H^\pm$ . The most important production mechanism for the neutral SUSY Higgs bosons at the Large Hadron Collider (LHC) is the gluon fusion mechanism,  $pp \rightarrow gg \rightarrow h^0, H^0, A^0$  [2], and the Higgs radiation off top and bottom quarks [3]. Except for the small range in the parameter space where the heavy neutral Higgs  $H^0$  decays into a pair of  $Z$  bosons, the rare  $\gamma\gamma$  decay mode, apart from  $\tau\tau$  decays, is a promising mode to detect the neutral Higgs particles, since  $b$  quarks are hard to separate from the QCD background. It has been pointed out [4, 5] that the lightest Higgs could be detected in this mode for sufficiently large values of the mass of the pseudoscalar Higgs boson  $m_A \gg m_Z$ . The  $\gamma\gamma$  channel is also important for the discovery of  $H^0$  for  $50 \text{ GeV} \leq m_A \leq 150 \text{ GeV}$ .

<sup>1</sup>To appear in: *Proceedings of Xth International Workshop: High Energy Physics and Quantum Field Theory*, Zvenigorod, Russia, September 20–26, 1995

<sup>2</sup>Permanent address: North Eastern Hill University, Laitumkrah, Shillong 793003, India.

Here we present results of a recent study [6] of the hadronic production and subsequent two-photon decay of the  $CP$ -even Higgs bosons ( $h^0$  and  $H^0$ ) of the MSSM, which is valid for the LHC energy of  $\sqrt{s} = 14$  TeV, using gluon distribution functions based on recent HERA data [7], in order to reassess the feasibility of observing the  $CP$ -even Higgs bosons in this mode. After the completion of this work, a related study was presented by Kane et al. [8]. As mentioned earlier, the gluon fusion mechanism is the dominant production mechanism of SUSY Higgs bosons in high-energy  $pp$  collisions throughout the entire Higgs mass range. We study the cross section for the production of the  $h^0$  and  $H^0$ , and their decays, taking into account all the parameters of the Supersymmetric Standard Model. In particular, we take into account the mixing in the squark sector, the chiral mixing. This also affects the Higgs boson masses through appreciable radiative corrections, and was previously shown to lead to large corrections to the rates [9].

In the calculation of the production of the Higgs through gluon-gluon fusion, we include in the triangle graph all the squarks, as well as  $b$  and  $t$  quarks, the lightest quarks having a negligible coupling to the  $h^0$ . On the other hand, in the calculation of decay of the Higgs to two photons, we include in addition to the above, all the sleptons,  $W^\pm$ , charginos and the charged Higgs boson.

An important role is played in our analysis by the bilinear Higgs coupling  $\mu$ , which occurs in the Lagrangian through the term

$$\mathcal{L} = \left[ -\mu \hat{H}_1^T \epsilon \hat{H}_2 \right]_{\theta\theta} + \text{h.c.}, \quad (1)$$

where  $\hat{H}_1$  and  $\hat{H}_2$  are the Higgs superfields with hypercharge  $-1$  and  $+1$ , respectively. Furthermore, the Minimal Supersymmetric Model contains several soft supersymmetry-breaking terms. We write the relevant soft terms in the Lagrangian as follows [10]

$$\begin{aligned} \mathcal{L}_{\text{Soft}} = & \left\{ \frac{gm_d A_d}{\sqrt{2} m_W \cos \beta} Q^T \epsilon H_1 \tilde{d}^R - \frac{gm_u A_u}{\sqrt{2} m_W \sin \beta} Q^T \epsilon H_2 \tilde{u}^R + \text{h.c.} \right\} \\ & - \tilde{M}_U^2 Q^\dagger Q - \tilde{m}_U^2 \tilde{u}^{R\dagger} \tilde{u}^R - \tilde{m}_D^2 \tilde{d}^{R\dagger} \tilde{d}^R - M_{H_1}^2 H_1^\dagger H_1 - M_{H_2}^2 H_2^\dagger H_2 \\ & + \frac{M_1}{2} \{ \lambda \lambda + \bar{\lambda} \bar{\lambda} \} + \frac{M_2}{2} \sum_{k=1}^3 \{ \Lambda^k \Lambda^k + \bar{\Lambda}^k \bar{\Lambda}^k \}, \end{aligned} \quad (2)$$

with subscripts  $u$  (or  $U$ ) and  $d$  (or  $D$ ) referring to up and down-type quarks. The Higgs production cross section and the two-photon decay rate depend significantly on several of these parameters. We shall in particular focus on the dependence on the trilinear couplings  $A_d$  and  $A_u$ .

The Higgs production cross section and the two-photon decay rate depend on the gaugino and squark masses, the latter being determined by, apart from the soft-supersymmetry breaking trilinear coefficients ( $A_u$ ,  $A_d$ ) and the Higgsino mixing parameter  $\mu$ , the soft supersymmetry-breaking masses, denoted in eq. (2) by  $\tilde{M}_U$ ,  $\tilde{m}_U$  and  $\tilde{m}_D$ , respectively. For simplicity, we shall consider the situation where  $\tilde{M}_U = \tilde{m}_U = \tilde{m}_D \equiv \tilde{m}$ , with  $\tilde{m}$  chosen to be 150 GeV for the first two generations, and varied over the values 150, 500 and 1000 GeV for the third generation.

The contributions of the squark and Higgs bosons to the decay rate depend on the relative sign between the parameters  $A$  and  $\mu$ , but not on their overall signs. We note that the Higgs sector depends on  $A$  and  $\mu$  through radiative corrections. The chargino contribution is independent of  $A$ , but depends on the relative sign between  $\mu$  and  $M_2$ . Thus, the  $h^0 \rightarrow \gamma\gamma$  decay rate is independent of the overall signs of  $A$ ,  $\mu$  and  $M_2$ , but depends on all the relative signs of these parameters. In most of the parameter space, however, the dependence on the chargino mass (and therefore on the sign of  $M_2$ ) is rather weak. In these regions it suffices to consider  $A$  positive and vary the sign of  $\mu$ . Finally, the signs of the off-diagonal terms in the squark mass matrices are determined by the definition of  $A$  and  $\mu$ , and also by the definition of the fermion masses [6].

In Sec. 2, we shall study the implications of the nonzero values of  $A$  and  $\mu$  on the Higgs masses, together with the constraints related to the other relevant masses. We shall then go on to study the cross sections and decay rates for the lighter and the heavier  $CP$ -even Higgs bosons in Secs. 3 and 4, respectively.

## 2 The Parameter Space

In this section we describe in detail the parameter space relevant for the production and decay of the lightest Higgs boson at LHC, and the theoretical and experimental constraints on it before presenting cross sections and decay rates.

At the tree level, the masses of the  $CP$ -even neutral Higgs bosons are given by ( $m_{h^0} \leq m_{H^0}$ ) [11]

$$m_{H^0, h^0}^2 = \frac{1}{2} \left[ m_A^2 + m_Z^2 \pm \sqrt{(m_A^2 + m_Z^2)^2 - 4m_Z^2 m_A^2 \cos^2 2\beta} \right], \quad (3)$$

which are controlled by two parameters,  $m_A$  (the mass of the  $CP$ -odd Higgs boson) and  $\tan \beta$  ( $= v_2/v_1$ , where  $v_2$  and  $v_1$  are the vacuum expectation values of the two Higgs doublets). Indeed, the entire Higgs sector at the tree level can be described in terms of these two parameters alone. The corresponding eigenstates are

$$H^0 = \sqrt{2} [(\text{Re } H_1^0 - v_1) \cos \alpha + (\text{Re } H_2^0 - v_2) \sin \alpha], \quad (4)$$

$$h^0 = \sqrt{2} [-(\text{Re } H_1^0 - v_1) \sin \alpha + (\text{Re } H_2^0 - v_2) \cos \alpha], \quad (5)$$

where  $H_1^0$  and  $H_2^0$  are the neutral components of the two Higgs doublets  $H_1$  and  $H_2$ , respectively. The  $CP$ -even mixing angle  $\alpha$  is defined through

$$\cos 2\alpha = -\cos 2\beta \left( \frac{m_A^2 - m_Z^2}{m_{H^0}^2 - m_{h^0}^2} \right), \quad -\frac{\pi}{2} \leq \alpha \leq 0. \quad (6)$$

There are, however, substantial radiative corrections [12] to the  $CP$ -even neutral Higgs masses. In the one-loop effective potential approximation, the radiatively corrected squared mass matrix for the  $CP$ -even Higgs bosons has the following form:

$$M^2 = \begin{pmatrix} \sin^2 \beta m_A^2 + \cos^2 \beta m_Z^2 & -\sin \beta \cos \beta (m_A^2 + m_Z^2) \\ -\sin \beta \cos \beta (m_A^2 + m_Z^2) & \cos^2 \beta m_A^2 + \sin^2 \beta m_Z^2 \end{pmatrix} + \begin{pmatrix} \Delta_{11} & \Delta_{12} \\ \Delta_{21} & \Delta_{22} \end{pmatrix}, \quad (7)$$

where the radiative corrections  $\Delta_{ij}$  depend on, besides the top quark mass, the bilinear parameter  $\mu$  in the superpotential, the soft supersymmetry breaking trilinear couplings ( $A_u$ ,  $A_d$ ), and masses ( $\tilde{M}_U$ ,  $\tilde{m}_U$ ,  $\tilde{m}_D$ , etc.), as well as  $\tan \beta$ . In the limit of no mixing,  $\mu = A_u = A_d = 0$ , so that  $\Delta_{11} = \Delta_{12} = \Delta_{21} = 0$ , with

$$\Delta_{22} = \frac{3g^2 m_t^4}{8\pi^2 m_W^2 \sin^2 \beta} \log \left( 1 + \frac{\tilde{m}^2}{m_t^2} \right), \quad \mu = A_u = A_d = 0. \quad (8)$$

The radiative corrections are, in general, positive, and they shift the mass of the lightest neutral Higgs boson upwards [12]. More recent radiative corrections to the Higgs sector [13] which are valid when the squark masses are of the same order of magnitude, have not been taken into account in our study [6]. As long as the “loop particles” are far from threshold for real production, the cross section does not depend very strongly on the exact value of the Higgs mass.

In order to simplify the calculations, we shall assume that all the trilinear couplings are equal so that

$$A_u = A_d \equiv A. \quad (9)$$

Furthermore, we shall take the top-quark mass to be 176 GeV [14] in our numerical calculations. The parameters that enter the neutral  $CP$ -even Higgs mass matrix are varied in the following ranges:

$$\begin{aligned} 50 \text{ GeV} &\leq m_A \leq 1000 \text{ GeV}, & 1.1 \leq \tan \beta \leq 50.0, \\ 50 \text{ GeV} &\leq |\mu| \leq 1000 \text{ GeV}, & 0 \leq A \leq 1000 \text{ GeV}. \end{aligned} \quad (10)$$

These values cover essentially the entire physically interesting range of parameters in the MSSM. However, not all of the above parameter values are allowed because of the experimental constraints on the squark, chargino and  $h^0$  masses. For low values of  $\tilde{m}$ , the lightest squark tends to be too light (below the most rigorous experimental bound of  $\sim 44.5$  GeV [15]), or even unphysical (mass squared negative). The excluded region of the parameter space is shown in the left part of fig. 1 for  $\tilde{m} = 150$  GeV,  $M_2 = 200$  GeV,

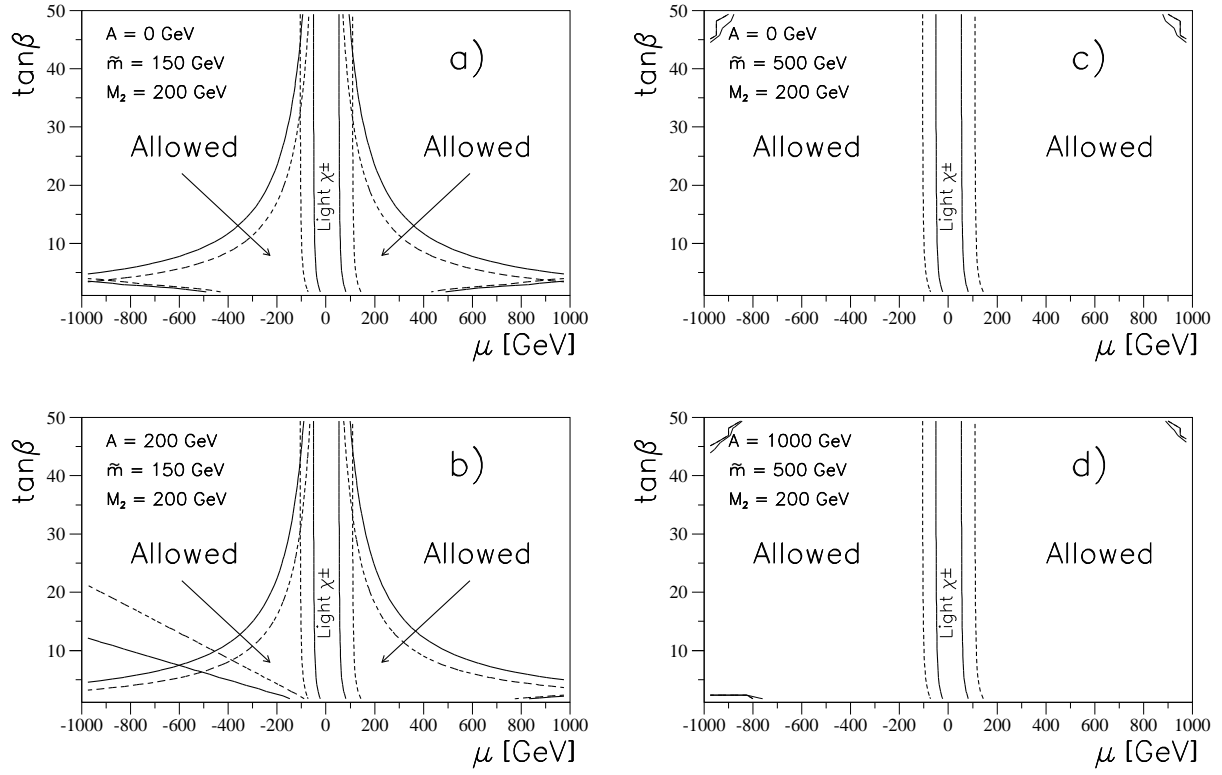


Figure 1. Regions in the  $\mu$ - $\tan\beta$  plane which are ruled out by too light chargino ( $\chi^\pm$ ), squark and Higgs masses. The gaugino mass scale is  $M_2 = 200$  GeV and  $m_A = 200$  GeV. The solid (dashed) contours for small  $|\mu|$  refer to the chargino mass  $m_{\chi^\pm} = 45$  (90) GeV. Two values of  $\tilde{m}$  are considered, left:  $\tilde{m} = 150$  GeV, right:  $\tilde{m} = 500$  GeV. Two values of the trilinear mixing parameter  $A = 0$  are considered: a) and c)  $A = 0$ , b)  $A = 200$  GeV, and d)  $A = 1000$  GeV. For  $\tilde{m} = 150$  GeV, the squark masses are too light or unphysical in much of the  $\mu$ - $\tan\beta$  plane. The hyperbola-like contours give regions that are excluded by the lightest  $b$  squark being below 45 GeV (solid) or 90 GeV (dashed). The more straight contours at large  $\mu$  and small  $\tan\beta$  similarly indicate regions that are excluded by the lightest  $t$  squark. For  $\tilde{m} = 500$  GeV the unlabelled contours near the corners at large  $|\mu|$  refer to regions where the  $h^0$  mass would be below 45 GeV.

$m_A = 200$  GeV and for two values of the trilinear coupling  $A$ . The allowed region in the  $\mu - \tan\beta$  plane decreases with increasing  $A$ , but the dependence on  $M_2$  and  $m_A$  in this region is rather weak. In order to have acceptable  $b$ -squark masses,  $\mu$  and  $\tan\beta$  must lie *inside* of the hyperbola-shaped curves. Similarly, in order to have acceptable  $t$ -squarks, the corners at large  $|\mu|$  and small  $\tan\beta$  must be excluded.

The chargino masses are, at the tree level, given by the expression

$$m_{\chi^\pm}^2 = \frac{1}{2}(M_2^2 + \mu^2) + m_W^2 \pm \left[ \frac{1}{4}(M_2^2 - \mu^2)^2 + m_W^4 \cos^2 2\beta + m_W^2(M_2^2 + \mu^2 + 2\mu M_2 \sin 2\beta) \right]^{1/2}. \quad (11)$$

For  $\mu = 0$ , we have

$$m_{\chi^\pm}^2 = \frac{1}{2}M_2^2 + m_W^2 \pm \left[ \frac{1}{4}M_2^4 + m_W^2 \cos^2 2\beta + m_W^2 M_2^2 \right]^{1/2}. \quad (12)$$

When  $\mu = 0$ , we see that, for  $\tan\beta \gg 1$ , the lightest chargino becomes massless. Actually, small values of  $\mu$  are unacceptable for all values of  $\tan\beta$ . The lowest acceptable value for  $|\mu|$  will depend on  $\tan\beta$ , but that dependence is rather weak. The excluded region due to the chargino being too light, increases with decreasing values of  $M_2$ . We note that the radiative corrections to the chargino masses are small for most of the parameter space [16]. In fig. 1 we show the contours in the  $\mu$ - $\tan\beta$  plane outside of which

the chargino has an acceptable mass ( $> 45$  GeV) [17]. By the time the LHC starts operating, one would have searched for charginos with masses up to 90 GeV at LEP2. Contours relevant for LEP2 are also shown.

For larger values of  $\tilde{m}$  (right part of fig. 1), there is no problem with the squark masses. However, for large values of  $\tilde{m}$  the experimental constraints on the  $h^0$  mass rule out some of the regions of parameter space. This is illustrated in fig. 1 for  $\tilde{m} = 500$  GeV. The corners at large values of  $|\mu|$  and  $\tan\beta$  must be excluded since one of the squarks there would be unphysical or the  $h^0$  mass would be lower than the experimental bound obtained at LEP [18]. The extent of these forbidden regions in the parameter space grow rapidly as  $m_A$  decreases below  $\mathcal{O}(150$  GeV). They also increase with increasing values of  $A$ .

As discussed above, the mass of the lighter  $CP$ -even Higgs boson  $h^0$  will depend significantly on  $\mu$ ,  $\tan\beta$ ,  $A$  and  $\tilde{m}$ , through the radiative corrections. For  $\tilde{m} = 500$  GeV, and two values each of  $m_A$  (100 and 200 GeV) and  $A$  (0 and 1000 GeV), the dependence on  $\mu$  and  $\tan\beta$  is displayed in fig. 2. As already indicated in fig. 1, at large  $|\mu|$  and large  $\tan\beta$ , the radiative corrections are large and negative, driving the value of  $m_{h^0}$  well below the tree-level value.

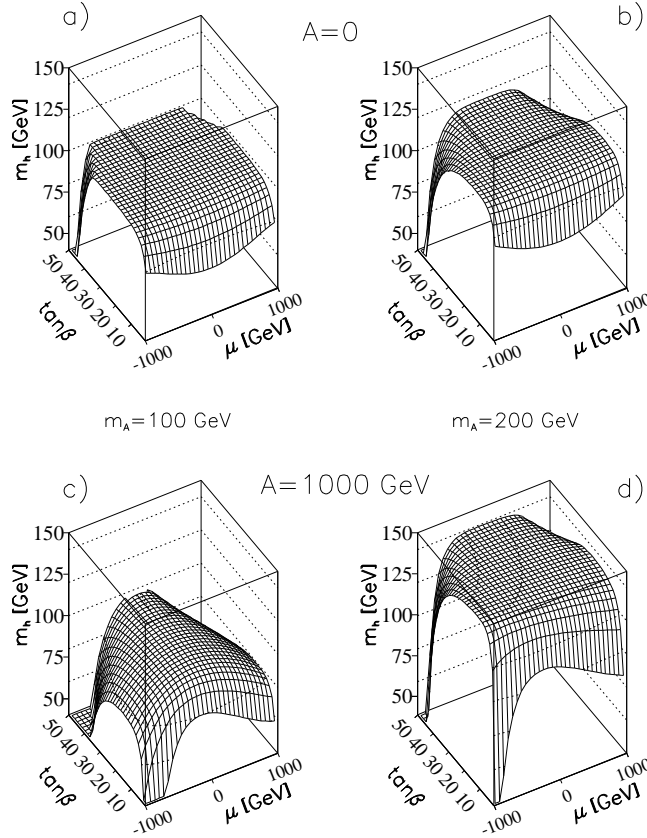


Figure 2. Mass of the lightest  $CP$ -even Higgs boson vs.  $\mu$  and  $\tan\beta$ , for  $M_2 = 200$  GeV and  $\tilde{m} = 500$  GeV. Two values of  $m_A$  and two values of  $A$  are considered: a)  $m_A = 100$  GeV,  $A = 0$ , b)  $m_A = 200$  GeV,  $A = 0$  GeV, c)  $m_A = 100$  GeV,  $A = 1000$  GeV, d)  $m_A = 200$  GeV,  $A = 1000$  GeV.

The charged Higgs boson mass is given by

$$m_{H^\pm}^2 = m_W^2 + m_A^2 + \Delta, \quad (13)$$

where  $\Delta$  arises due to radiative corrections and is a complicated function of the parameters of the model [19].

The radiative corrections to the charged Higgs mass are, in general, not as large as in the case of neutral Higgs bosons. This is due to an approximate global  $SU(2) \times SU(2)$  symmetry [20], valid in the limit of no mixing. In certain regions of parameter space the radiative corrections can, however, be large.

This is the case when the trilinear mixing parameter  $A$  is large,  $m_A$  is small, and when furthermore  $\tan\beta$  is large. We shall include the effects of non-zero  $A$  and  $\mu$  in the calculation of the charged Higgs mass. The present experimental lower bound of 40–45 GeV [21] on the charged Higgs is not restrictive, but presumably by the time the LHC starts operating, one will have searched for charged Higgs bosons at LEP2 with mass up to around 90 GeV. Even this bound does not appreciably restrict the parameter space.

The neutralino mass matrix depends on the four parameters  $M_2$ ,  $M_1$ ,  $\mu$  and  $\tan\beta$ . However, one may reduce the number of parameters by assuming that the MSSM is embedded in a grand unified theory so that the SUSY-breaking gaugino masses are equal to a common mass at the grand unified scale. At the electroweak scale, we then have [22]

$$M_1 = \frac{5}{3} \tan^2 \theta_W M_2. \quad (14)$$

We shall assume this relation throughout in what follows. The neutralino masses enter the calculation through the total width of the Higgs boson. We have considered values of the gaugino mass parameter  $M_2$  to be 50, 200, or 1000 GeV [6]. We shall here present the numerical results for the case of  $M_2 = 200$  GeV. The experimental constraint on the lightest neutralino mass rules out certain regions of the parameter space [23], but these depend on several parameters, and are therefore not reproduced in fig. 1. They are generally correlated with the bounds on chargino masses [17].

### 3 The lighter $CP$ -even Higgs boson $h^0$

The cross section for

$$pp \rightarrow h^0 X, \quad (15)$$

is calculated from the triangle diagram convoluted with the gluon distribution functions,

$$\sigma = \sqrt{2} \pi G_F \left( \frac{\alpha_s}{8\pi} \right)^2 \frac{m_{h^0}^2}{s} \left| \sum_k I_k(\tau) \right|^2 \int_{-\log(\sqrt{s}/m_{h^0})}^{\log(\sqrt{s}/m_{h^0})} dy G\left(\frac{m_{h^0}}{\sqrt{s}} e^y\right) G\left(\frac{m_{h^0}}{\sqrt{s}} e^{-y}\right), \quad (16)$$

with contributions from various diagrams  $k$ . For the standard case of a top-quark loop,

$$I(\tau) = \frac{\tau}{2} \left\{ 1 - (\tau - 1) \left[ \arcsin\left(\frac{1}{\sqrt{\tau}}\right) \right]^2 \right\}, \quad (17)$$

and  $\tau = (2m_t/m_{h^0})^2 > 1$ .

For  $M_2 = 200$  GeV,  $\tilde{m} = 500$  GeV, and  $\mu = 500$  GeV, we show in fig. 3 this cross section for four values of  $A$ , the trilinear coupling parameter. From this figure the following features are noteworthy:

- The cross section decreases appreciably for large values of  $A$ . This is mainly due to an increase in the  $h^0$  mass.
- The cross section increases sharply for small values of  $\tan\beta$ , and also at small  $m_A$ . The increase at small  $\tan\beta$  is caused by the  $h^0$  becoming light. At small values of  $m_A$  and large  $A$ , the couplings of  $h^0$  to  $b$  quarks and  $\tau$  leptons become large, making the cross section very large in this region.

For the same parameters as above, we show in fig. 4 the total decay rate,  $\Gamma(h^0 \rightarrow \text{all})$  and the two-photon decay rate,  $\Gamma(h^0 \rightarrow \gamma\gamma)$ . In contrast to fig. 3, here we only consider two values of  $A$ , namely  $A = 0$  and  $A = 1000$  GeV. The two-photon decay rate is seen to increase sharply at large values of  $A$ , but this does not result in a correspondingly larger rate for the process

$$pp \rightarrow h^0 X \rightarrow \gamma\gamma X, \quad (18)$$

since the production cross section also decreases, as shown in fig. 3 (mostly due to an increase in the Higgs mass,  $m_{h^0}$ ). In fig. 5 we show the cross section for the process (18). A characteristic feature of the cross section is that it is small at moderate values of  $m_A$ , and then increases steadily with increasing

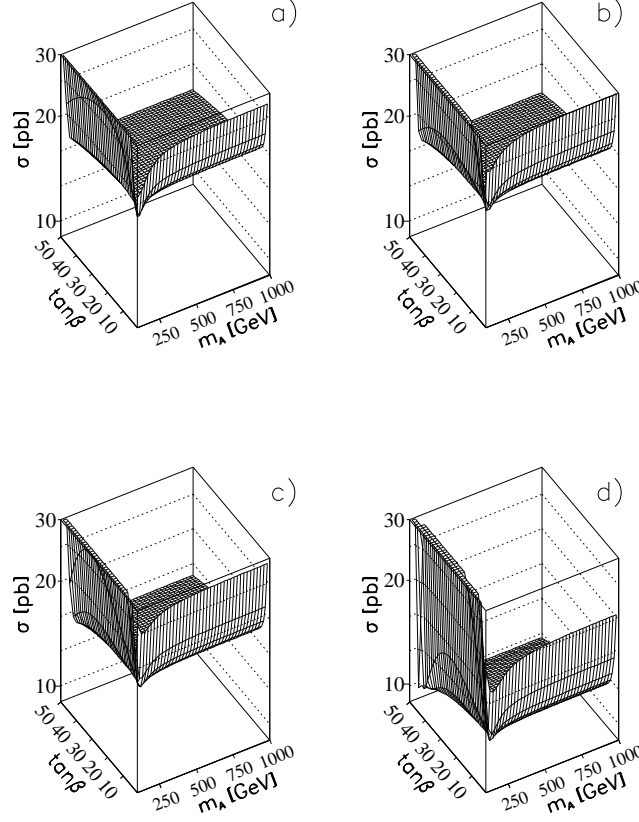


Figure 3. Cross section for  $pp \rightarrow h^0 X$  as a function of  $m_A$  and  $\tan \beta$  for  $M_2 = 200$  GeV,  $\tilde{m} = 500$  GeV, and  $\mu = 500$  GeV. Four values of  $A$  are considered: a)  $A = 0$ , b)  $A = 200$  GeV, c)  $A = 500$  GeV and d)  $A = 1000$  GeV.

$m_A$ , reaching asymptotically a plateau. This behaviour is caused by the contribution of the  $W$  to the triangle graph for  $h^0 \rightarrow \gamma\gamma$ . The  $h^0 WW$  coupling is proportional to  $\sin(\beta - \alpha)$ , where<sup>3</sup>

$$\cos^2(\beta - \alpha) = \frac{m_{h^0}^2(m_Z^2 - m_{h^0}^2)}{m_{A^0}^2(m_{H^0}^2 - m_{h^0}^2)}. \quad (19)$$

For large  $m_A$ , at fixed  $\beta$ , all Higgs masses, except  $m_{h^0}$ , become large, so that  $h^0$  decouples. For large  $m_A$ , we actually have  $\sin(\beta - \alpha) \rightarrow 1$ , which is why the cross section increases and reaches a plateau for large  $m_A$ . For these values of  $\tilde{m}$  and  $\mu$  (fig. 5), the increase in  $A$  leads to larger cross sections over most of the  $m_A$ - $\tan \beta$  plane.

If we use Higgs masses as given in ref. [13], the cross section exhibits less variation with  $A$ . But this comparison is incomplete since those masses are not valid for large  $A$  where the squark mass splitting is large.

The  $\mu$ -dependence of the cross section can for the case of  $M_2 = 200$  GeV and  $\tilde{m} = 500$  GeV be described as follows. At moderate values ( $\mu = \pm 200$  GeV), there is not much difference between the cross section for positive and negative values of  $\mu$ . The cross section has a significant dependence on  $m_A$ , being low at  $m_A \leq \mathcal{O}(300 \text{ GeV})$ , then increasing steadily and reaching a plateau with increasing  $m_A$ . The dependence on  $\tan \beta$  is rather weak. In [6] we show more details in contour plots of the cross section (18), for  $M_2 = 200$  GeV,  $\tilde{m} = 500$  GeV and  $\mu$  equal to  $\pm 500$ .

For increasing values of  $|\mu|$  (500 GeV, 1000 GeV) the change in the cross section is rather complex. This is illustrated by figures 6–8, and is basically caused by two phenomena: (1) At large values of  $|\mu|$  some squarks become too light or unphysical, in analogy with the case ( $M_2 = 200$  GeV,  $\tilde{m} = 150$  GeV)

<sup>3</sup>In actual calculations we take the radiatively corrected formula for  $\alpha$ .

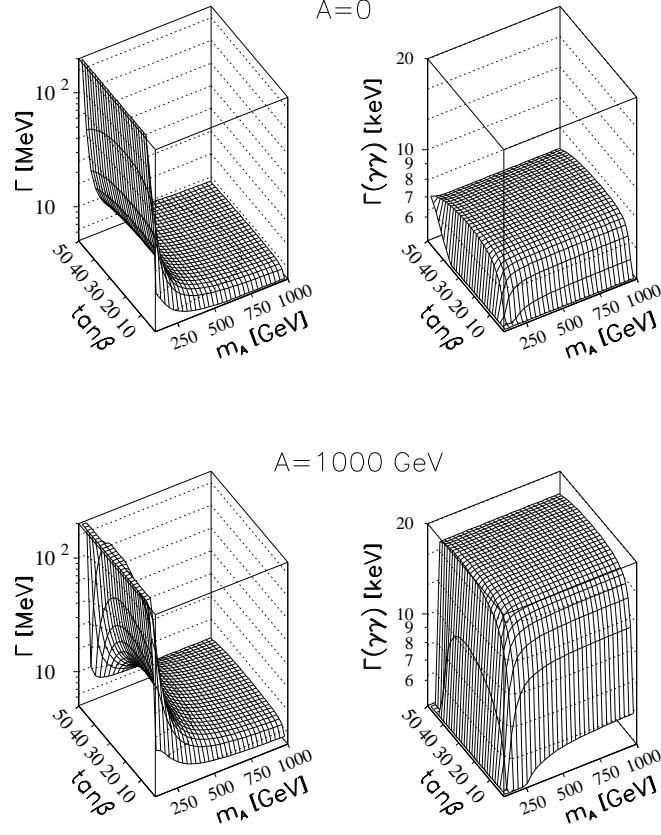


Figure 4. Total decay rate  $\Gamma(h^0 \rightarrow \text{all})$  and two-photon decay rate  $\Gamma(h^0 \rightarrow \gamma\gamma)$ , as functions of  $m_A$  and  $\tan\beta$  for  $M_2 = 200$  GeV,  $\tilde{m} = 500$  GeV, and  $\mu = 500$  GeV. Two values of  $A$  are considered:  $A = 0$  and  $A = 1000$  GeV.

shown in fig. 1. Hence, there are regions both at small and large values of  $\tan\beta$  where the cross section is not defined. (2) At large values of  $|\mu|$  and large values of  $\tan\beta$  (all  $m_A$ ) the Higgs gets very light (due

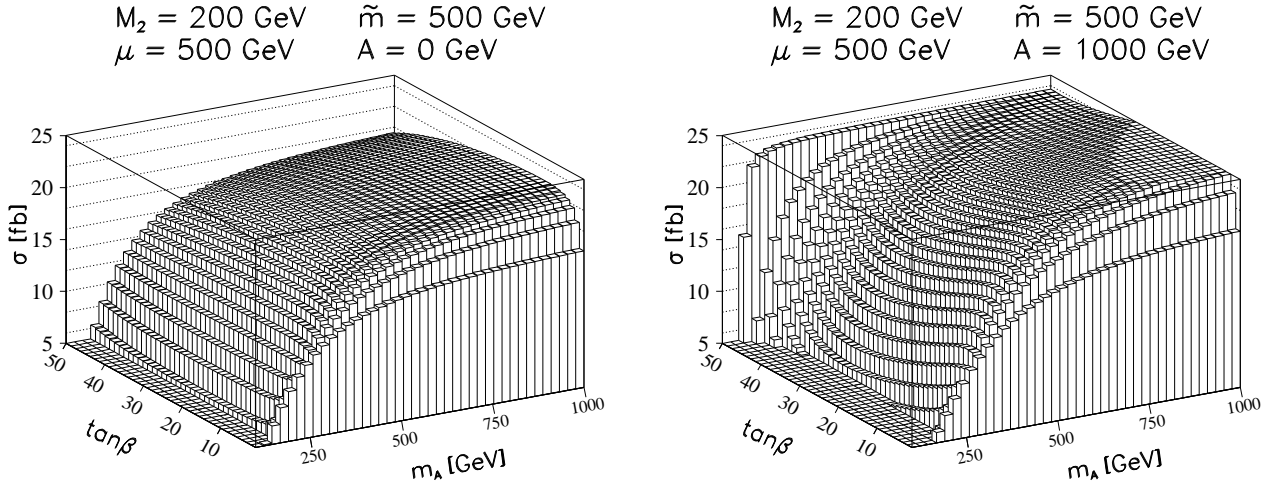


Figure 5. Cross section for  $pp \rightarrow h^0 X \rightarrow \gamma\gamma X$  as a function of  $m_A$  and  $\tan\beta$  for  $M_2 = 200$  GeV,  $\tilde{m} = 500$  GeV,  $\mu = 500$  GeV, and two values of  $A$ : left:  $A = 0$ , right:  $A = 1000$  GeV.



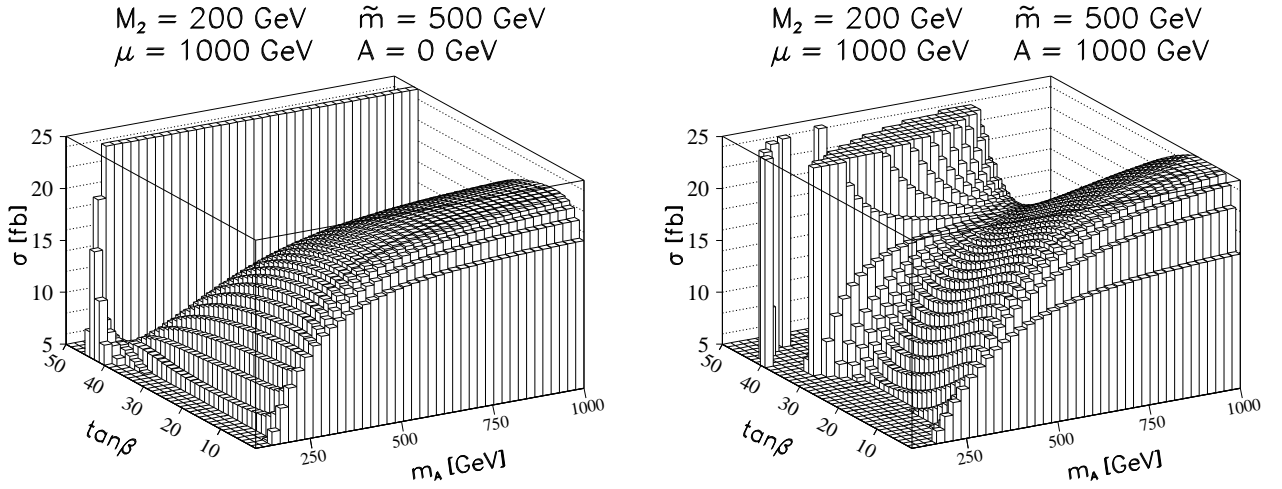


Figure 6. Cross section for  $pp \rightarrow h^0 X \rightarrow \gamma\gamma X$  as a function of  $m_A$  and  $\tan\beta$  for  $M_2 = 200$  GeV,  $\tilde{m} = 500$  GeV,  $\mu = 1000$  GeV, and two values of  $A$ : left:  $A = 0$ , right:  $A = 1000$  GeV.

to radiative corrections, see fig. 2).

As a consequence of (2), the cross section can get rather high, where not forbidden due to (1) above. However, the two-photon decay rate, which is typically dominated by the  $W$ -loop contribution, also depends on the Higgs mass. In fact, the contribution of the  $W$ -loop to the decay amplitude is proportional to [11]

$$\frac{\sin(\beta - \alpha)}{\tau} [2 + 3\tau + 3\tau(2 - \tau)f(\tau)], \quad (20)$$

with  $\tau = (2m_W/m_{h^0})^2$  and  $f(\tau)$  the usual ‘triangle function’

$$f(\tau) = \begin{cases} \left[ \arcsin\left(\frac{1}{\sqrt{\tau}}\right) \right], & \tau \geq 1, \\ -\left[ -\cosh^{-1}\left(\frac{1}{\sqrt{\tau}}\right) + \frac{i\pi}{2} \right]^2, & \tau < 1. \end{cases} \quad (21)$$

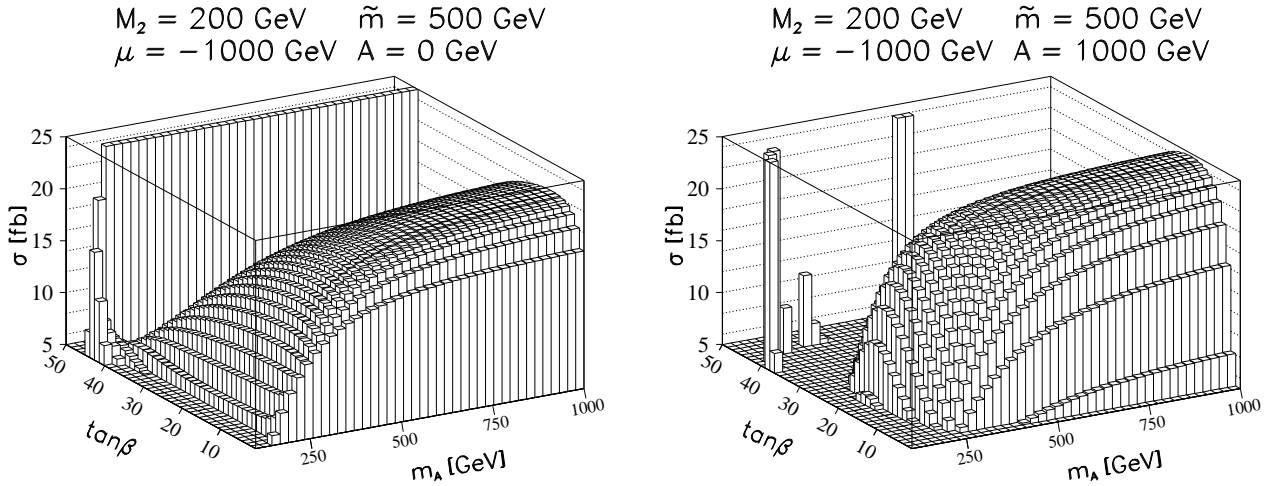


Figure 7. Cross section for  $pp \rightarrow h^0 X \rightarrow \gamma\gamma X$  as a function of  $m_A$  and  $\tan\beta$  for  $M_2 = 200$  GeV,  $\tilde{m} = 500$  GeV, and  $\mu = -1000$  GeV. left:  $A = 0$ , right:  $A = 1000$  GeV.

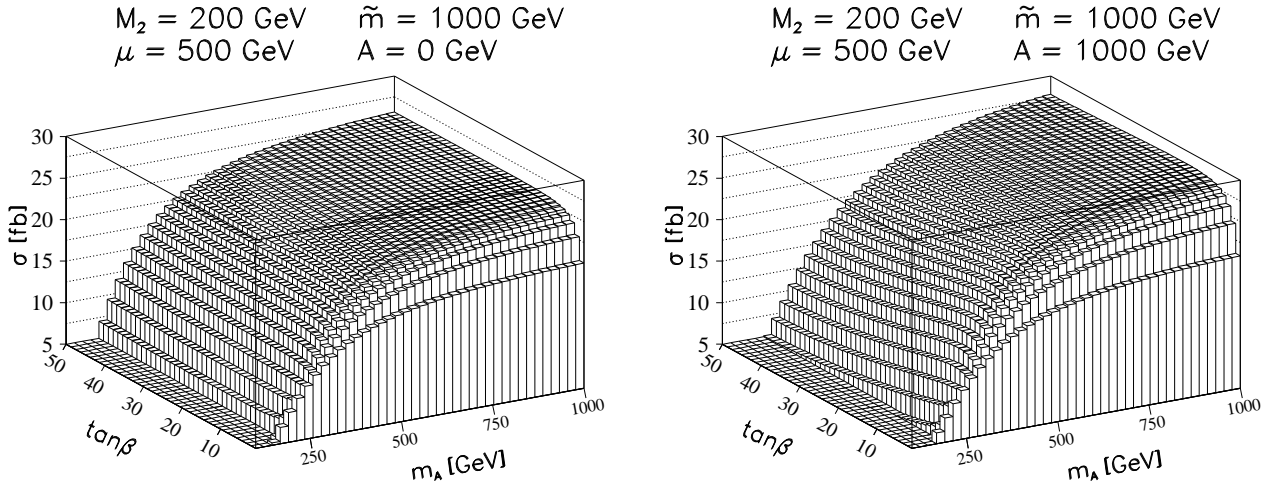


Figure 8. Cross section for  $pp \rightarrow h^0 X \rightarrow \gamma\gamma X$  as a function of  $m_A$  and  $\tan\beta$  for  $M_2 = 200$  GeV,  $\tilde{m} = 1$  TeV, and  $\mu = 500$  GeV. left:  $A = 0$ , right:  $A = 1000$  GeV.

In fact, the decrease of this function (20) explains the decrease in the cross section multiplied by the branching ratio, as seen in figs. 6 and 7 for large values of  $\tan\beta$  where  $m_{h^0}$  becomes small, cf. fig. 2. (The coupling factor  $\sin(\beta - \alpha)$  remains close to 1 for practically the whole range of  $\tan\beta$ , provided  $m_A$  is not too small.<sup>4</sup>) Finally, the secondary *increase* seen in figs. 5 and 6 at large values of  $\tan\beta$  and large  $A$  is due to an increase in the two-photon branching ratio. (The total decay rate falls off faster at large values of  $\tan\beta$  than the two-photon decay rate.)

The dependence of the cross section on  $M_2$  and  $\tilde{m}$  is described in table 1 of ref. [6]. For small values of  $\tilde{m}$  ( $\sim 150$  GeV), the possible ranges of  $\tan\beta$ ,  $\mu$  and  $A$  become severely restricted, when requiring physically acceptable squark masses. There is a significant increase in the cross section as  $\tilde{m}$  increases from 500 GeV to 1 TeV, to values of the order of 25–30 fb (see fig. 8). At this large value of  $\tilde{m}$ , the dependence on  $\mu$ ,  $A$  and  $\tan\beta$  becomes weaker.

For small values of  $M_2$  ( $\sim 50$  GeV), the allowed range in  $\mu$  must be restricted in order to obtain physically acceptable chargino masses. As  $M_2$  *increases* beyond 200 GeV, there is little further change in the cross section.

The cross section has a modest dependence on the choice of gluon distribution function used. For the plots shown here, we have used the recent GRV Set 3 [25] distributions, which are the default of the PDFLIB. Other sets lead to variations of the order of 5–10% [6]. These uncertainties are thus rather insignificant as compared to the dependence on the mixing parameters  $\mu$  and  $A$ .

## 4 The heavier $CP$ -even Higgs boson $H^0$

Finally, we consider the process

$$pp \rightarrow H^0 X \rightarrow \gamma\gamma X, \quad (22)$$

which is of interest for small values of  $m_A$ .

The two-photon decay of the heavier  $CP$ -even Higgs boson  $H^0$  proceeds dominantly through the  $W$  loop, and its amplitude is proportional to  $\cos(\beta - \alpha)$ . It is, thus, complementary to the decay of the lighter  $CP$ -even Higgs boson  $h^0$ , whose coupling to a pair of  $W$  bosons is proportional to  $\sin(\beta - \alpha)$ . It is significant only if  $m_A$  is small, which means  $m_{H^0}$  itself is light, since<sup>5</sup>, from eqs. (7) and (8), we have

<sup>4</sup>For a discussion of these parameters, see also ref. [24].

<sup>5</sup>In numerical calculations, we use the complete one-loop radiatively corrected formula for  $m_{H^0}$  with non-zero values of  $\mu$ ,  $A_u$  and  $A_d$ .

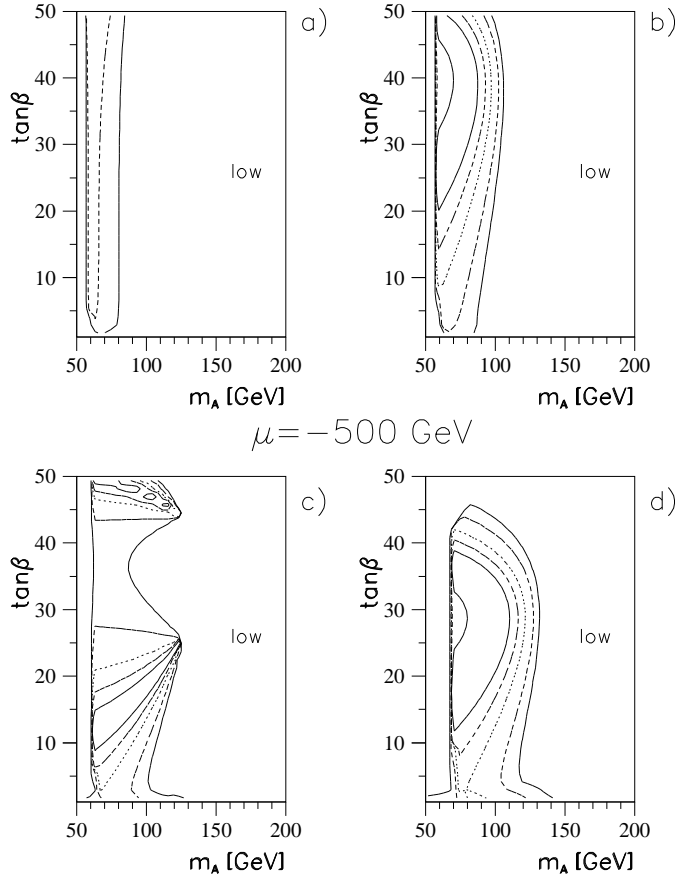


Figure 9. Dependence of the  $pp \rightarrow H^0 \rightarrow \gamma\gamma$  cross section on  $m_A$  and  $\tan\beta$  for different values of the trilinear couplings  $A$ . Four values of  $A$  are considered: a)  $A = 0$ , b)  $A = 200$  GeV, c)  $A = 500$  GeV and d)  $A = 1000$  GeV. Here  $M_2 = 200$  GeV,  $\tilde{m} = 500$  GeV, and  $\mu = -500$  GeV. The contours are at 10 fb (solid), 20 fb, 50 fb, 100 fb and 200 fb.

(for  $\mu = A_u = A_d = 0$ )

$$m_{H^0}^2 = m_{A^0}^2 + m_Z^2 - m_{h^0}^2 + \Delta_{22}. \quad (23)$$

At small values of  $m_A$ , the total  $H^0$  decay rate is small and thus, there can be considerable branching ratio for it to go into two photons. As a result, the cross section for the process (22) at small values of  $m_A$  can be as large as 200 fb or even more. In fig. (9) we show the contour plot of the cross section for the process (22) for  $\mu = -500$  GeV, and for four different values of  $A$ . For this value of  $\mu$ , there is a strong increase in the cross section with increasing values of  $A$ . On the other hand, for positive values of  $\mu$ , increasing the value of  $A$  leads to a decrease in the cross section. This is shown in fig. (10), where we plot the cross section for  $\mu = 500$  GeV. At low values of  $m_A$  the Higgs mass  $m_{H^0}$  is of the order of 110–140 GeV, and the  $h^0$  mass is close to the experimental lower limit.

## 5 Summary and concluding remarks

We have discussed in detail the cross section for the production of  $CP$ -even Higgs bosons at the LHC, in conjunction with their decay to two photons. Where the parameters lead to a physically acceptable phenomenology, the cross section multiplied by the two-photon branching ratio for the lighter  $CP$ -even Higgs boson is of the order of 20–30 fb.

Similar results have been presented in [8]. Within the context of a SUGRA GUT model, these authors consider basically a random sample of parameters compatible with experimental and theoretical constraints. The cross sections obtained in [8] appear to be somewhat higher than those of [6].

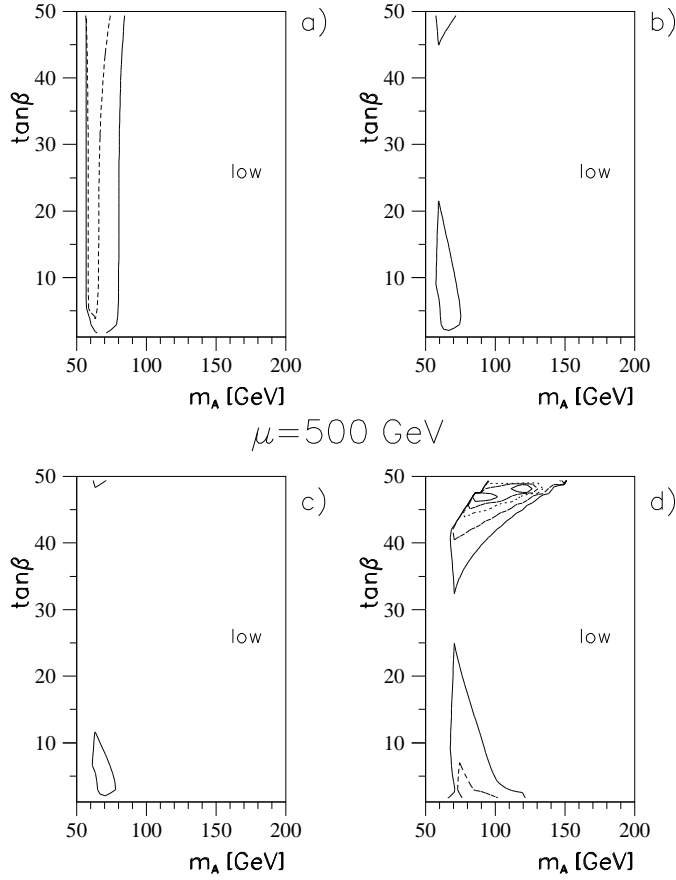


Figure 10. Dependence of the  $pp \rightarrow H^0 \rightarrow \gamma\gamma$  cross section on  $m_A$  and  $\tan\beta$  for different values of the trilinear couplings  $A$ . As in fig. 9, except that  $\mu = 500$  GeV.

These calculations do not take into account QCD corrections. Such corrections have been evaluated for the quark-loop contribution, and lead to enhancements of the cross section of about 50% [26]. However, in the presence of chiral mixing the squark loops also contribute significantly. Since the QCD corrections for these are not available, we have not considered the higher-order QCD effects here. One should, of course, keep in mind that they are very important.

There is a modest increase of the cross section with increasing values of  $A$  (i.e., with increasing chiral mixing). This comes about as the result of two competing effects: with increasing  $A$ , the Higgs boson becomes more heavy, leading to lower production cross sections. This is however offset by a corresponding increase in the two-photon decay rate.

It is a pleasure to thank the Organizers of the Zvenigorod Workshop, in particular Professor V. Savrin, for creating a very stimulating and pleasant atmosphere during the meeting. This research has been supported by the Research Council of Norway. PNP would like to thank Alexander von Humboldt-Stiftung and Prof. H.J.W. Müller-Kirsten for support while this paper was written. The work of PNP is supported by the Department of Science and Technology under project No. SP/S2/K-17/94.

## References

- [1] H.-P. Nilles, Phys. Rep. C110 (1984) 1;  
H. E. Haber and G. L. Kane, Phys. Rep. C117 (1985) 75;  
R. Barbieri, Riv. Nuovo Cimento 11 (1988) No. 4, p. 1;  
For a recent review, see, e.g., R. Arnowitt and P. Nath, Lecture at Swieca School, Campos do

- Jordao, Brazil, 1993; in *Sao Paulo 1993*, Proceedings, Particles and fields, 3-63; CTP-TAMU-93-052 and NUB-TH-3073-93, hep-ph/9309277.
- [2] H. M. Georgi, S. L. Glashow, M. E. Machacek, and D. V. Nanopoulos, Phys. Rev. Lett. 40 (1978) 692.
  - [3] Z. Kunszt, Nucl. Phys. B247 (1984) 339;  
W.J. Marciano and F.E. Paige, Phys. Rev. Lett. 66 (1991) 2433;  
J.F. Gunion, Phys. Lett. B261 (1991) 510.
  - [4] Z. Kunszt and F. Zwirner, Nucl. Phys. B385 (1992) 3.
  - [5] H. Baer, M. Bisset, C. Kao and X. Tata, Phys. Rev. D46 (1992) 1067;  
V. Barger, M.S. Berger, A.L. Stange and R.J.N. Phillips, Phys. Rev. D45 (1992) 4128;  
J.F. Gunion and L.K. Orr, Phys. Rev. D46 (1992) 2052;  
V. Barger, Kingman Cheung, R.J.N. Phillips and A.L. Stange, Phys. Rev. D46 (1992) 4914.
  - [6] B. Kileng, P. Osland and P.N. Pandita, NORDITA preprint 95/48 P; hep-ph/9506455, Zeitschrift f. Physik, in press;  
University of Bergen, Department of Physics Scientific/Technical Report No. 1995-13, ISSN 0803-2696; Contributed paper, *International Euophysys Conference on High Energy Physics*, Brussels, Belgium, July 27 – August 2 1995 and *17th International Symposium on Lepton-Photon Interactions*, August 10–15, 1995, Beijing, China.
  - [7] H. Plothow-Besch, PDFLIB (CERNLIB), version 4.17; Comp. Phys. Comm. 75 (1993) 396.
  - [8] G.L. Kane, G.D. Kribs, S.P. Martin, J.D. Wells, hep-ph/9508265.
  - [9] B. Kileng, Zeitschrift f. Physik, C63 (1994) 87.
  - [10] L. Girardello and M.T. Grisaru, Nucl. Phys. B194 (1982) 65; see also ref. [9].
  - [11] J.F. Gunion, H.E. Haber, G. Kane and S. Dawson, *The Higgs Hunter's Guide*, Addison-Wesley, 1990.
  - [12] Y. Okada, M. Yamaguchi, T. Yanagida, Prog. Theor. Phys. 85 (1991) 1; Phys. Lett. B262 (1991) 54;  
J. Ellis, G. Ridolfi and F. Zwirner, Phys. Lett. B257 (1991) 83; Phys. Lett. B262 (1991) 477;  
H.E. Haber and R. Hempfling, Phys. Rev. Lett. 66 (1991) 1815.
  - [13] M. Carena, J.R. Espinosa, M. Quiros and C.E.M. Wagner, Phys. Lett. B355 (1995) 209.
  - [14] CDF Collaboration, F. Abe, et al., Phys. Rev. Lett. 73 (1994) 225; *ibid.* 74 (1995) 2626;  
D0 Collaboration, S. Abachi, et al., Phys. Rev. Lett. 74 (1995) 2632.
  - [15] DELPHI Collaboration, P. Abreu et al., Phys. Lett. B247 (1990) 148;  
OPAL Collaboration, R. Akers et al., Phys. Lett. B337 (1994) 207.
  - [16] D. Pierce and A. Papadopoulos, Phys. Rev. D50 (1994) 565; Nucl. Phys. B430 (1994) 278;  
A.B. Lahanas, K. Tamvakis and N.D. Tracas, Phys. Lett. B324 (1994) 387.
  - [17] ALEPH Collaboration, D. Decamp, et al., Phys. Lett. B236 (1990) 86.
  - [18] ALEPH Collaboration, D. Buskulic, et al., Phys. Lett. B313 (1993) 312.
  - [19] A. Brignole, J. Ellis, G. Ridolfi and F. Zwirner, Phys. Lett. B271 (1991) 123;  
A. Brignole, Phys. Lett. B277 (1992) 313;  
M.A. Diaz and H.E. Haber, Phys. Rev. D45 (1992) 4246.
  - [20] H.E. Haber and A. Pomarol, Phys. Lett. B302 (1993) 435.
  - [21] ALEPH Collaboration, D. Buskulic, et al., Phys. Lett. B241 (1990) 623.
  - [22] K. Inoue, A. Kakuto, H. Komatsu, S. Takeshita, Prog. Theor. Phys. 68(1982) 927, Erratum *ibid.* 70 (1983) 330; *ibid.* 71 (1984) 413.
  - [23] R. Barbieri, G. Gamberini, G.F. Giudice and G. Ridolfi, Phys. Lett. 195B (1987) 500;  
J. Ellis, G. Ridolfi and F. Zwirner, Phys. Lett. 237B (1990) 423.
  - [24] A. Djouadi, J. Kalinowski and P.M. Zerwas, Z. Phys. C57 (1993) 569.
  - [25] M. Glück, E. Reya and A. Vogt Z. Phys. C53 (1992) 127.
  - [26] M. Spira, A. Djouadi, D. Graudenz and P.M. Zerwas, Nucl. Phys. B453 (1995) 17.